Supporting Information for

The magnetopyroelectric effect: Heat-mediated magnetoelectricity in magnetic nanoparticle-ferroelectric polymer composites

*Joaquin Llacer-Wintle[a], Jan Renz[a], Lukas Hertle[a], Andrea Veciana[a], Denis von Arx[a], Jiang Wu[a], Pere Bruna[b], Marija Vukomanovic[c], Josep Puigmartí-Lui[d], Bradley J. Nelson[a], Xiang-Zhong Chen[*a], Salvador Pané[*a]*

[a]Multi-Scale Robotics Lab (MSRL), Institute of Robotics and Intelligent Systems (IRIS), ETH Zurich, CH-8092 Zurich, Switzerland.

[b]Departament de Física, Universitat Politècnica de Catalunya, BarcelonaTech (UPC); Institut de Tècniques Energètiques (INTE); Barcelona Research Center in Multiscale Science and Engineering, Av. Eduard Maristany 16, 08019 Barcelona, Spain

[c]Biomaterials group, Advanced Materials Department, Jožef Stefan Institute, 1000 Ljubljana, Slovenia.

[d]Departament de Ciència dels Materials i Química Física, Institut de Química Teòrica i Computacional, 08028 Barcelona, Spain; Institució Catalana de Recerca i Estudis Avançats (ICREA), 08010 Barcelona, Spain.

Email: chenxian@ethz.ch, vidalp@ethz.ch.

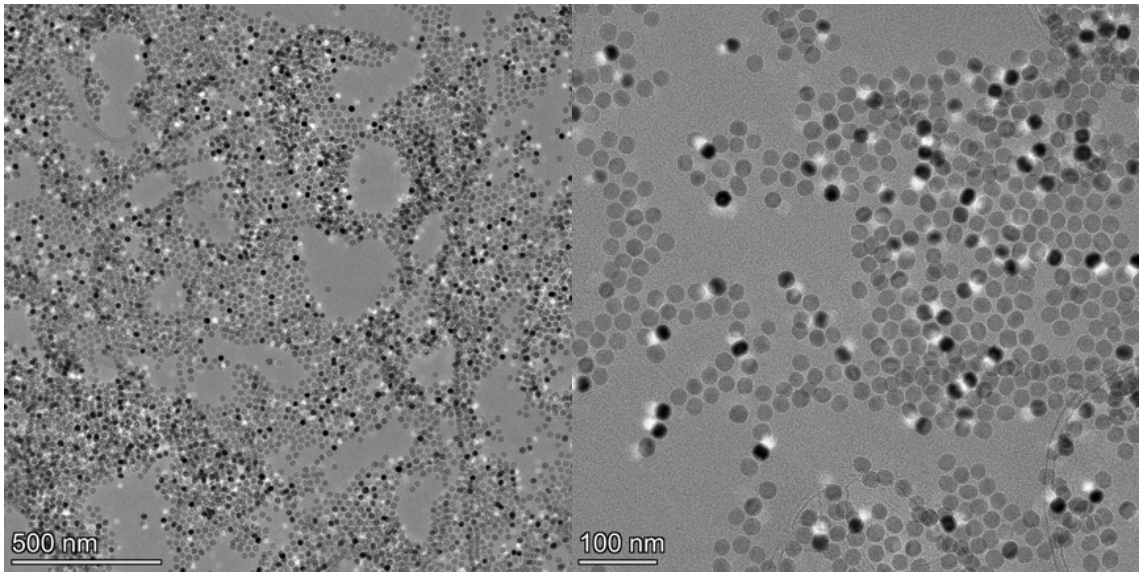

Figure S1. Transmission electron microscopy of the IONPs.

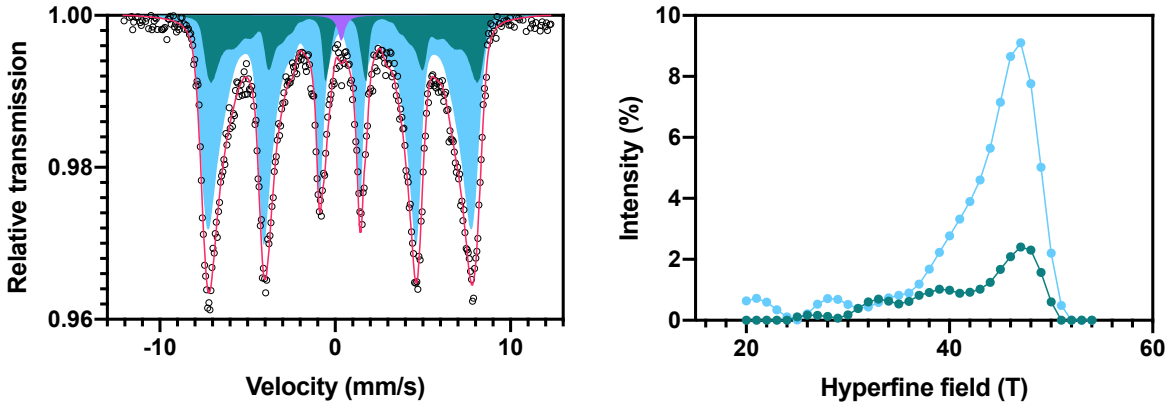

Figure S2. (Left) Room temperature Mössbauer spectrum of the IONPs. The black circles represent the experimental data, the red line is the total fit and the shaded areas represent the three subspectral components (two distributions of sextets and one singlet). (Right) The corresponding distributions of the magnetic hyperfine fields are plotted using the same colors. **Interpretation of the Mössbauer data:** The spectra of the sample was fitted using two hyperfine field distributions for the ferromagnetic part of the spectra. [L. P. Ferreira *et. al.*, 2022] In this case, a paramagnetic singlet is also needed to obtain a good fit in the central part. Figure S2 shows (Left) the experimental spectra with the best fit curve and (Right) the two distributions of hyperfine fields. The width of the peaks indicates the presence of a distribution of hyperfine fields, i.e., slightly different environs surroundings the Fe atoms. In this fitting method, two distributions have been used for two different iron sites. The distribution with a higher amount of Fe (colored in light blue) presents a value of the isomer shift of ~0.28 (1) mm s-1 and a quadrupole splitting of ~0.0 (1) mm s-1, typical to Fe^{3+} sites, while the other distribution (colored in dark green) has values of the isomer shift of ~0.54 (1) mm s-1 and fixed quadrupole splitting of ~-0.09 mm s-1. These parameters are typical of $Fe^{2.5+}$, a mixture of Fe^{2+} and Fe^{3+} in magnetite.[L. P. Ferreira *et. al.*, 2022] The atomic percentage of each iron environment is 77 at.% for the first distribution and 22 at.% for the second, showing that the relative amount of Fe^{3+} and $Fe^{2.5+}$ is not the one corresponding to the usual occupations of

tetrahedral and octahedral iron sites in magnetite. Therefore, the iron sites assigned to Fe^{3+} correspond to a mixture of magnetite and maghemite or magnetite with a certain degree of oxidation. The broad hyperfine field distributions are indicative of a distribution of the nanoparticle sizes and the need to use components with low values of the magnetic field (specially between 30 and 40 T) could be explained by some degree of structural defects. Finally, the fitting is not complete without a paramagnetic singlet to take into account the central part of the spectra. This component accounts for an 1 at% of Fe atoms and it can be associated with a wüstite phase, although its low amount makes difficult the determination of its hyperfine parameters and its precise characterization.

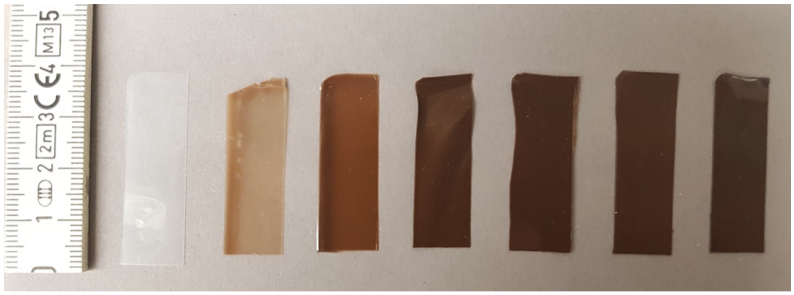

Figure S3. Composite films with different loading of IONPs. From left to right: 0, 0.3, 1.3, 2.6, 3.9, 5.1, 11.9 wt%.

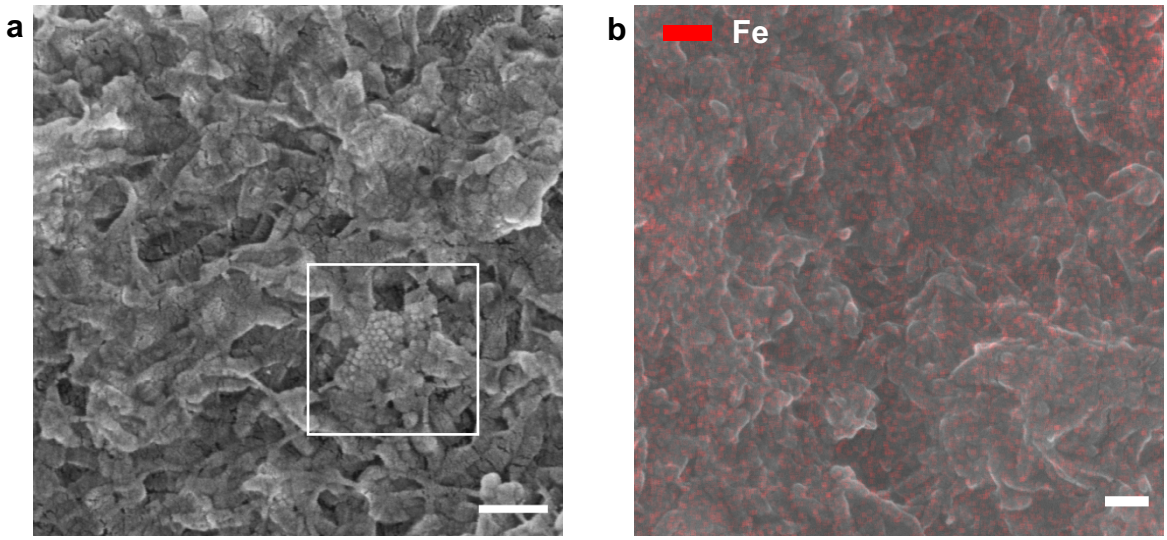

Figure S4. (a) A small cluster of IONPs, showing that the structure of the individual IONPs is preserved. Note that due to the granular texture of the PVDF-TrFE, small clusters of IONPs are easier to identify than individual nanoparticles. (b) An SEM-EDX image of the cross-section of a typical composite film shows a good distribution of IONPs in the sample. Scale bars: 250 nm.

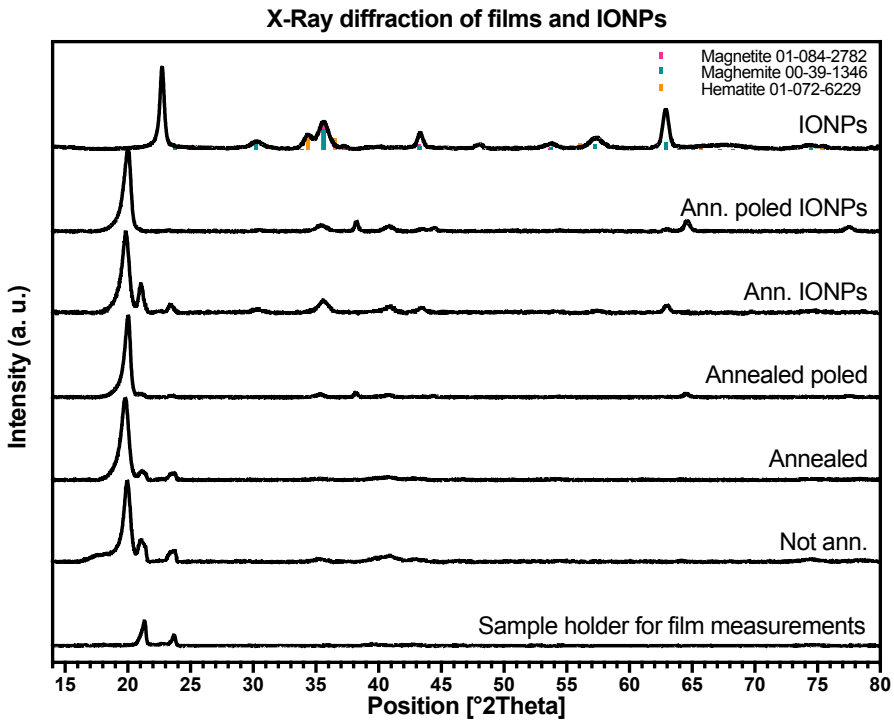

Figure S5. X-ray diffraction of the films and IONPs. The sample holder used to measure the films was measured as a control.

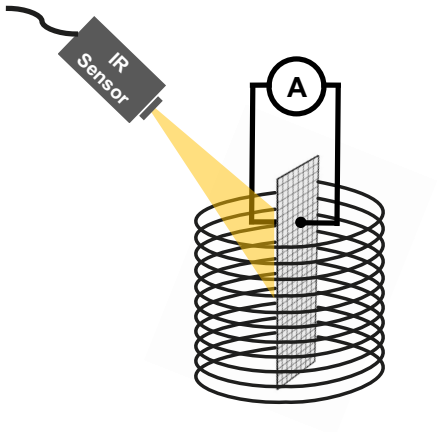

Figure S6. Schematic of the magnetopyroelectric measuring setup.

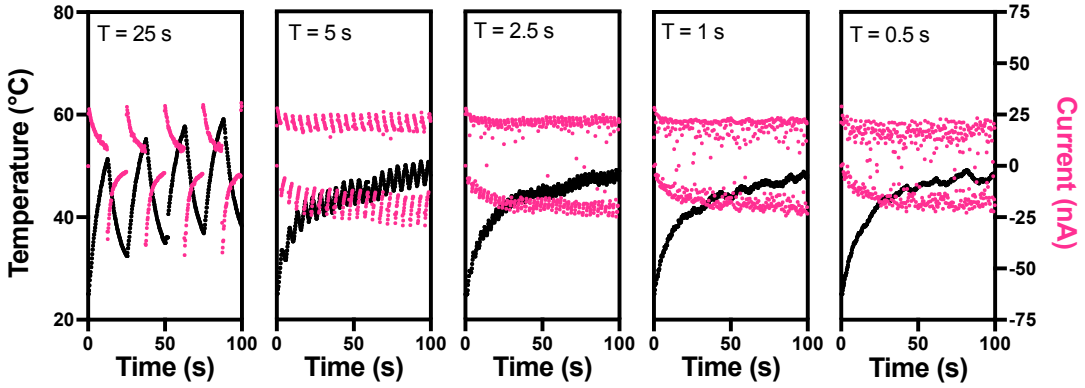

Figure S7. Effect of the magnetic pulse period on MPE.

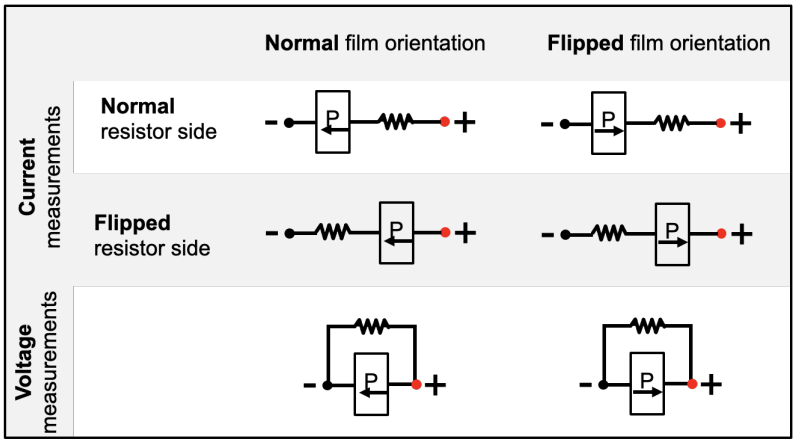

Figure S8. Schematic of the electrical circuit integrating the MPE film. The P and the arrow represent the polarization direction of the film. The black and red nodes represent the corresponding negative and positive connections to the electrometer.

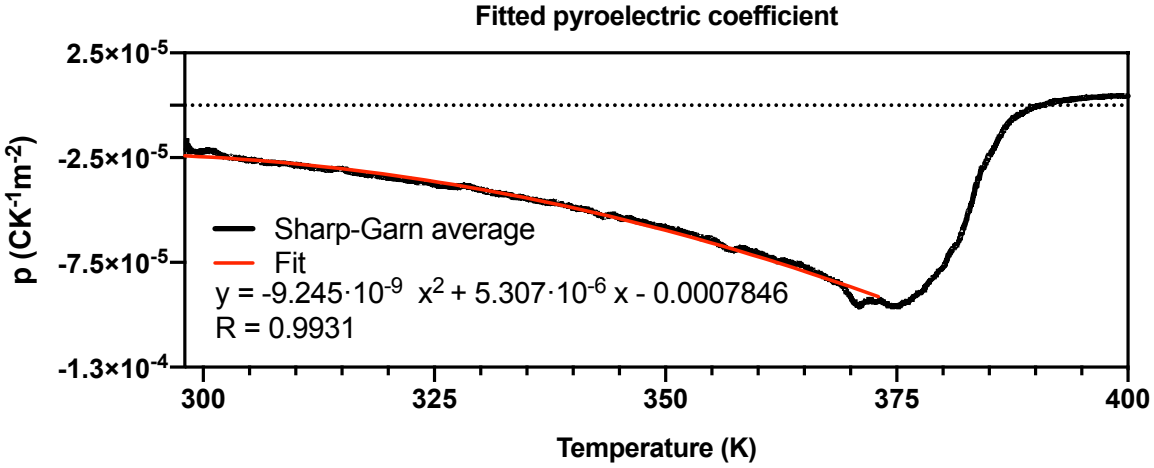

Figure S9. Quadratic fit of the pyroelectric coefficient as a function of temperature (300-370 K) measured via the Sharp-Garn method.

Appendix S1. A simple model to simulate magnetopyroelectricity

Definitions			
Property	**Variable**	**Unit**	**Value**
Density P(VDF-TrFE) 70-30 (ref. 30)	ρ	kg/m³	1940
Heat capacity at constant pressure P(VDF-TrFE) 70-30 (ref. 30)	C_p	J/(kg·K)	1170
Heat capacitance	C	J/K	54.475E-3
Specific Loss Power of IONPs	SLP	W/g	273
Total mass of IONPs (11.9 wt%)	m_{IONPs}	g	6.089E-3
Heating efficiency	α	-	0.14 (Best match)
Heat transfer coefficient	h	W/(m2·K)	12 (From fit SI Table 1)
Heat transfer surface area	A_h	m^2	2 x 30E-3 x 8 E-3
Environment temperature	T_{env}	K	298 K
Initial temperature	T_0	K	298 K
Electrode area	A_I	m^2	30E-3 x 8 E-3
Pyroelectric coefficient	$p(T)$	C/(m^2·K)	(From fit Figure S9)

The internal energy (U) of an incompressible material is related by the heat capacitance of the body

$$\frac{dU}{dt} = C\frac{dT}{dt}$$

Because of energy conservation

$$\frac{dU}{dt} = \frac{dQ_{heating}}{dt} - \frac{dQ_{cooling}(T)}{dt}$$

Considering that the gained heat is only given by the specific loss power (SLP) of the constituting IONPs

$$\frac{dQ_{heating}}{dt} = SLP \cdot m_{IONPs} \cdot \alpha$$

and approximating the heat losses to Newton's law of cooling

$$\frac{dQ_{cooling}(T)}{dt} = h \cdot A_h \cdot (T(t) - T_{env})$$

The differential equation becomes

$$\frac{dT}{dt} = \frac{1}{C} \cdot \left(SLP \cdot m_{IONPs} \cdot \alpha - h \cdot A_h \cdot (T(t) - T_{env})\right)$$

The solution of the ordinary differential equation gives the temperature of the composite film as a function of time

$$T(t) = \frac{SLP \cdot m_{IONPs} \cdot \alpha}{h \cdot A_h} + T_{env} + C_1 \cdot e^{-\frac{A_h \cdot h}{C}t}$$

Solving for the initial condition ($T(t=0) = T_0$),

$$T(t) = T_{env} + \frac{SLP \cdot m_{IONPs} \cdot \alpha}{h \cdot A_h} + \left(T_0 - T_{env} - \frac{SLP \cdot m_{IONPs} \cdot \alpha}{h \cdot A_h}\right) \cdot e^{-\frac{A_h \cdot h}{C}t}$$

Where $\alpha = 0$ during cooling and $0 < \alpha < 1$ during heating.

Then, the temperature change rate is

$$\frac{dT(t)}{dt} = -\frac{A_h \cdot h}{C} \cdot \left(T_0 - T_{env} - \frac{SLP \cdot m_{IONPs} \cdot \alpha}{h \cdot A_h}\right) \cdot e^{-\frac{A_h \cdot h}{C}t}$$

The change in the spontaneous polarization of the film (in the polar direction) is then given by

$$dP_s = p(T) \cdot dT$$

And consequently, the generated pyroelectric current is

$$I_p = A_I \cdot p(T) \cdot \frac{dT}{dt}$$

Table S1. Calculated heat transfer coefficients from a one-phase decay fit of the cooling step [W/m^{2}K]						
Experiment ID	T0	Tenv	h	Standard error	R^2	df
11.9 wt%, T = 100	62.6	31.8	11.3	0.5305	0.9951	441
11.9 wt%, flipped, T = 100 s	66.7	31.7	11.7	0.4709	0.9970	441
11.9 wt%, T = 25	51.9	29.0	17.3	0.1565	0.9992	113

Table S2. Calculated heat transfer coefficients from a two-phase decay fit of the cooling step [W/m^{2}K]									
Experiment ID	T0	Tenv	h_{fast}	h_{slow}	RatioFast	$h_{weighed}$	Standard error	R^2	df
11.9 wt%, T = 100	64.5	28.8	20.0	4.3	0.574	13.3	0.1638	0.9995	439
11.9 wt%, flipped, T = 100 s	68.17	27.1	16.8	2.8	0.681	12.3	0.1068	0.9998	439
11.9 wt%, T = 25		unstable							

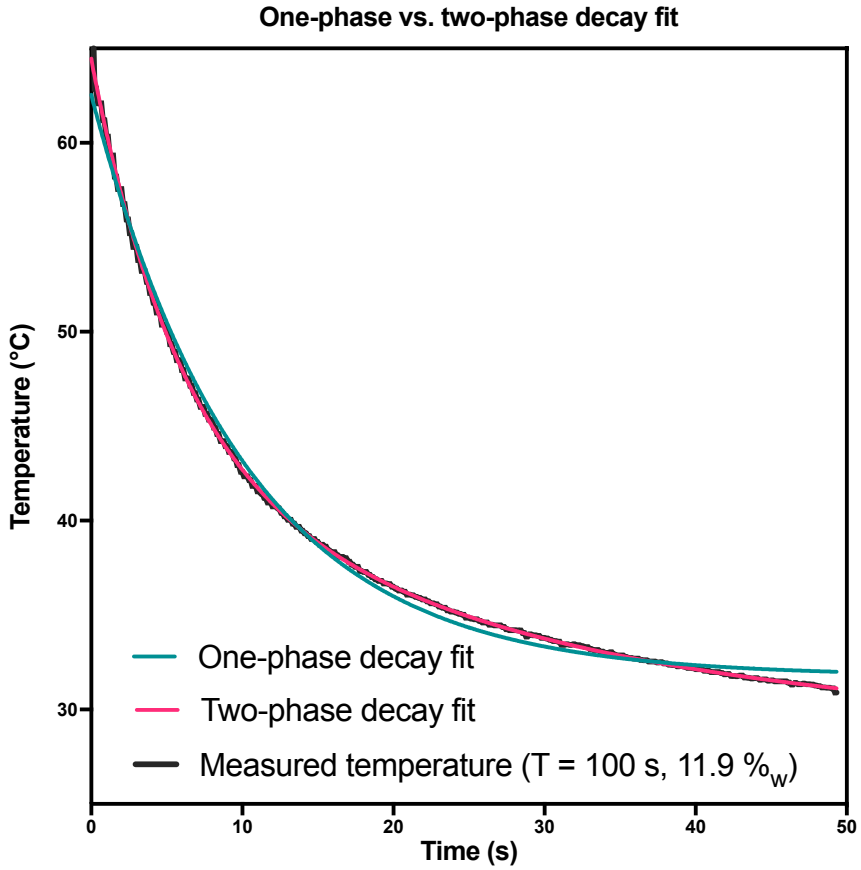

Figure S10. One and two-phase decay fitting of the temperature of a 11.9 wt% film during the first cooling step. The two-phase fit is more accurate.